CARBON 49 (2011) 1013–1017

available at www.sciencedirect.com

ScienceDirect

journal homepage: www.elsevier.com/locate/carbon

A density-functional theory simulation of the formation of Ni-doped fullerenes by ion implantation

Erik Neyts [a,*], *Axel Maeyens* [a], *Geoffrey Pourtois* [a,b], *Annemie Bogaerts* [a]

[a] *Department of Chemistry, PLASMANT Research Group, University of Antwerp, Universiteitsplein 1, B-2610 Wilrijk-Antwerp, Belgium*

[b] *IMEC, Kapeldreef 75, B-3001 Leuven, Belgium*

ARTICLE INFO

Article history:
Received 27 June 2010
Accepted 4 November 2010
Available online 13 November 2010

ABSTRACT

Using self-consistent Kohn–Sham density-functional theory molecular dynamics simulations, we demonstrate the theoretical possibility to synthesize NiC_{60}, the incarfullerene $Ni@C_{60}$ and the heterofullerene $C_{59}Ni$ in an ion implantation setup. The corresponding formation mechanisms of all three complexes are elucidated as a function of the ion implantation energy and impact location, suggesting possible routes for selectively synthesizing these complexes.

1. Introduction

Since their first discovery in 1985 [1], the synthesis and properties of metallofullerenes have been intensively studied because of their unique physical and chemical properties and potential applications, e.g. as electronic, optic and magnetic materials, as well as magnetic resonance imaging contrast agents and radiotracers in medical sciences [2–4]. Three types of complexes can be distinguished: (i) *incarfullerenes*, in which the dopant atom(s) are trapped inside the carbon cage (see, e.g. [5] and references therein); (ii) *metallofullerenes* where the metal atom is bound outside to the cage [6,7]; and (iii) *heterofullerenes* [8], in which the metal atom is incorporated into the cage network by replacing one or more C-atoms. Common production of metallofullerenes is by a DC electric arc discharge or a laser furnace method [5].

Alternatively, the ion implantation method has also been demonstrated to provide a viable route for the formation of doped fullerenes. In this process, the atoms to be complexed are ionized, accelerated, and implanted in the fullerene target. Anderson and co-workers demonstrated the implantation of rare gas ions and alkali metal ions into fullerene molecules using implantation energies in the range 0–150 eV [9–13]. Campbell and Hertel [14,15] investigated the formation of $M@C_{60}$ by bombarding thin films of C_{60} with M^+ alkali ions (M = Li, Na, K, and Rb). The formation of endohedral $^{133}Xe@C_{60}$ was reported by Watanabe et al. [16]. The implantation of Cs^+ in C_{60} was accomplished by Kaplan et al. using low energy ions (35–220 eV) [17]. The possibility to produce alkali metal or rare gas doped fullerenes by (low energy) ion implantation is therefore established experimentally.

To the authors' knowledge, only a few experimental papers are devoted to the study of the formation of first row transition metal doped fullerenes [18–21], in contrast to the abundant literature on the formation of complexes using rare earth metals and alkali and alkaline earth metals (see, e.g. [5,17,22,23] and references therein). The formation of the heterofullerene $C_{59}Ni$ from NiC_{60} was demonstrated experimentally by Branz et al. [19] and Kong et al. [20,21]. In these experiments, the heterohedral complexes were formed by photofragmentation from NiC_{60}. The structure of $C_{59}Ni$ was discussed in simulation papers by Sparta et al. [24], Changgeng et al. [25], and Alemany et al. [26]. The structure of the NiC_{60} complex was studied by Andriotis and Menon [27] and Alemany et al. [26]. The gas phase synthesis of an endohedral Ni containing fullerene has been simulated by Yamaguchi et al. using classical

* *Corresponding author:* Fax: +32 3 265 23 43.
E-mail address: erik.neyts@ua.ac.be (E. Neyts).
0008-6223/$ - see front matter
doi:10.1016/j.carbon.2010.11.009

molecular dynamics (MD) simulations [28]. Previously, we have also investigated the formation process of exo- and endohedral Ni–metallofullerene by classical MD simulations [29]. In this contribution, we present a more comprehensive study of the dynamical formation of various Ni-doped fullerenes by self-consistent density-functional theory (DFT) MD simulations corresponding to an ion implantation setup, including the first-time demonstration of the formation process of $C_{59}Ni$ (nica(C_{60}-Ih)[5,6]fullerene). Furthermore, new formation mechanisms of NiC_{60} (nickel(C_{60}-Ih)[5,6]fulleride) and $Ni@C_{60}$ ((C_{60}-Ih)[5,6]fullerene-incarnickel) are also presented.

2. Methodology

Density-functional theory calculations employing the self-consistent Kohn–Sham functional were performed using the SIESTA code [30,31]. The dynamic formation process was simulated by launching a Ni-atom with a predefined kinetic energy at a C_{60} molecule as outlined below. Subsequently, the coordinates of the obtained structures were optimized using the conjugate gradient (CG) minimization scheme.

In all calculations, a double-zeta basis set including polarization functions (DZP), the Perdew–Zunger local density approximation (LDA) exchange–correlation functional [32] and norm-conserving pseudopotentials including scalar relativistic effects according to the Troullier–Martins scheme were used [33,34]. The quality of the basis set has been carefully tested on both bulk nickel and on different carbon polymorphs. In each case, the structural and electronic properties of classical plane-wave simulations were faithfully reproduced. The cutoff radii r_c were set to 1.52 bohr for all C-orbitals, and to 2.67 bohr, 2.35 bohr, 2.13 bohr, and 2.13 bohr for *s*, *p*, *d* and *f* Ni-orbitals, respectively. The equivalent plane-wave cutoff for the fast Fourier transform grid (mesh cutoff) was set to 160 Ry. A cubic unit cell of 100 bohr × 100 bohr × 100 bohr was used to electronically isolate periodic images of the system and to prevent fast moving atoms to interact more than once with the target. The Fermi–Dirac occupation function with an electronic temperature corresponding to the physical system temperature (300 K) was used. The relative tolerance in the density matrix, taken as self-consistent field (SCF) convergence criterion, was set to 10^{-4} eV. The force tolerance in the minimization procedure was set to 0.01 eV/Å, during which no explicit symmetry constraints were imposed.

The simulation procedure is as follows. First, a C_{60} molecule which is thermalized with the Nose thermostat at 300 K is positioned in the simulation box. A Ni-atom is then launched at the C_{60} molecule normal to a specific location on the molecule with a predefined kinetic energy KE = {5 eV; 30 eV; 35 eV; 40 eV}. These energies were chosen based on our previous classical MD simulations [29]: between thermal energy and 10 eV, only the formation of NiC_{60} was observed in the simulation, while at 30 eV and 40 eV, both NiC_{60} and $Ni@C_{60}$ were formed. The chosen impact locations are (i) an atom (from hereon referred to as *top-site*), (ii) the center of a hexagon (*hex-site*), (iii) the center of a pentagon (*pen-site*), (iv) the center of a bond connecting two hexagons ("6–6 bond") (*66-site*), and (v) the center of a bond connecting a hexagon and a pentagon ("6–5 bond") (*65-site*). Each simulation therefore corresponds to a unique parameter pair {KE, location}. The trajectories of all atoms were integrated using the Verlet algorithm with a fixed time step of 1 fs in the microcanonical ensemble. The total integration time was set to 1 ps.

3. Results and discussion

An overview of the formed products is shown in Table 1. The formation mechanisms are described below. Note that due to the long calculation times (about 1 month per case), it is currently not possible to determine a probability distribution of the formed product vs. implantation energy.

3.1. *Formation of NiC_{60}*

NiC_{60} is observed to be formed by two distinct mechanisms: surface sticking and a *push-through* mechanism. In the case of surface sticking, the incoming Ni-atom has insufficient energy to break or sufficiently stretch any C–C bonds in order to enter the cage structure. Surface sticking is found to be operative only at 5 eV impacts, specifically at the *pen*, *6–6* and *6–5* impact locations. Previously, we have already demonstrated this mechanism by classical MD simulations [29]. At higher impact energy, however, we find a new mechanism to be operative, leading to the formation of these complexes. In this mechanism, the Ni-atom has sufficient energy to open the cage structure by breaking C–C bonds, travel through the cage and open the cage again at the side opposite to the impact location. Hence, the Ni-atom can reappear at the surface, thereby forming the NiC_{60} complex. The broken carbon–carbon bonds are swiftly reconnected after the impact. We term this formation process a push-through mechanism. An example of this mechanism is shown in Fig. 1 for the {pen, 35 eV} case. This mechanism is responsible for the majority of the formation of the NiC_{60} complexes (see Table 1).

Table 1 – Overview of the structures formed after the Ni-impact and subsequent energy minimization.

	Top	Hex	Pen	6–6	6–5
5 eV	No complex	Incar, closed	Exo (st, 5)	Exo (st, 6)	Exo (st, 5)
30 eV	Hetero	Exo (pt, 2)	Incar, closed	Incar, closed	Exo (pt, 5)
35 eV	Hetero	Exo (pt, 2)	Exo (pt, 6)	Incar, closed	Exo (pt, 6)
40 eV	Incar, open	Exo (pt, 5)	Incar, closed	Incar, closed	Incar, open

(st) denotes surface sticking, (pt) denotes push-through. "Exo" denotes the complex in which the Ni-atom is bound outside to the carbon cage. The number indicates the number of bonds formed between Ni and the buckyball.

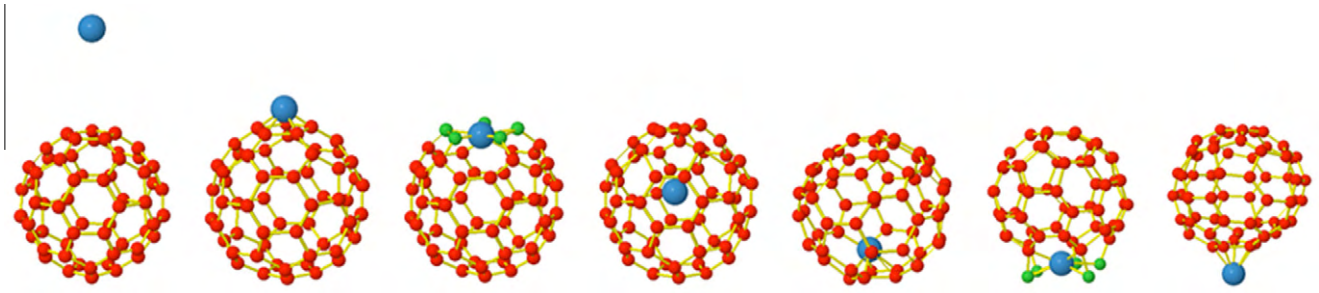

Fig. 1 – Push-through formation mechanism of a NiC_{60} complex for a 35 eV Ni-impact on the center of a pentagon of the buckyball, representative for all push-through formation mechanisms as listed in Table 1. The carbon atoms are color coded according to C–C coordination: gray = 0-coordinated; green = 1- or 2-coordinated; red = 3-coordinated; dark blue = 4-coordinated. The light blue big spheres represent Ni-atoms. (For interpretation of the references to color in this figure legend, the reader is referred to the web version of this article.)

Structurally, three different complexes can be distinguished. In four cases ({hex, 40 eV}, {pen, 5 eV}, {6–5, 5 eV}, and {6–5, 30 eV}), the Ni-atom binds on top of a pentagon with five Ni–C bonds of 2.02 Å each, corresponding to the "HS' site" in [26]. In [26], a bond length of 2.13 Å was obtained. In three cases ({pen, 35 eV}, {6–5, 35 eV}, and {6–6, 5 eV}), the Ni-atom binds to all six carbon atoms of a hexagon with a bond length of 2.07 Å, to be compared to the value of 2.15 Å obtained for the "HS site" in [26]. Previously, we have already detected the formation of both complexes [29]. In two cases, however, ({hex, 30 eV} and {hex, 35 eV}), the Ni-atom binds to two carbon atoms only, forming a bridge between two hexagons. This configuration corresponds to the "bridge site" in [25] and the "BS site" in [26]. The calculated Ni–C bond length of 1.825 Å lies in between the values of [27] (1.76 Å) and [26] (1.92 Å).

3.2. *Formation of $Ni@C_{60}$ and $Ni@C_{59}$*

Incarfullerenes are found to be formed upon impact on all sites and at all energies. The formed complex can consist of either an open cage or a closed cage. Again, two mechanisms can be distinguished. In all cases except {top, 40 eV}, the impinging Ni-atom breaks at least one C–C bond, creating a large ring big enough for the Ni-atom to enter the cage structure. Due to the initial bond breaking, the Ni-atom has lost sufficient energy such that it cannot escape the cage, thereby forming an incarfullerene. In all cases where this mechanism is operative, except the {6–5, 40 eV} case, the cage structure is regenerated after the initial impact. Fig. 2 shows the {hex, 5 eV} case as an example. In this particular case, the Ni-atom breaks three C–C bonds of the hexagon on which it is impinging, while leaving the other three intact. After the Ni-atom has entered the cage, the three broken C–C bonds are reconnected. This mechanism corresponds to the deformation/destruction mechanism described by Hirata et al. [35] for La-ion implantation in C_{60}. Note that bond breaking is already required for implanting ions as small as Na^+ and Ne^+ [10,11].

In the {top, 40 eV} simulation, a different, previously unobserved process is found. In this case, the impingement of the Ni-atom causes all three C–C bonds of the targetted C-atom to break. The targetted C-atom travels at high velocity through the cage, and in turn ejects another C-atom from the structure. Finally, the initially targetted C-atom replaces the ejected C-atom, while the Ni-atom binds to the inside of the damaged cage. The final structure is a defected $Ni@C_{59}$ complex, with two adjacent pentagons and an octagon.

3.3. *Formation of the heterofullerene $C_{59}Ni$*

The new mechanism described above for the formation of the incarfullerene $Ni@C_{59}$ complex is very similar to the mechanism for the formation of the heterofullerene $C_{59}Ni$ and is shown in Fig. 3. The Ni-atom pushes the targetted C-atom into the cage which in turn ejects a C-atom from the buckyball and replaces it. In the {top, 30 eV} and {top, 35 eV} simulations, however, the Ni-atom does not move into the cage, but

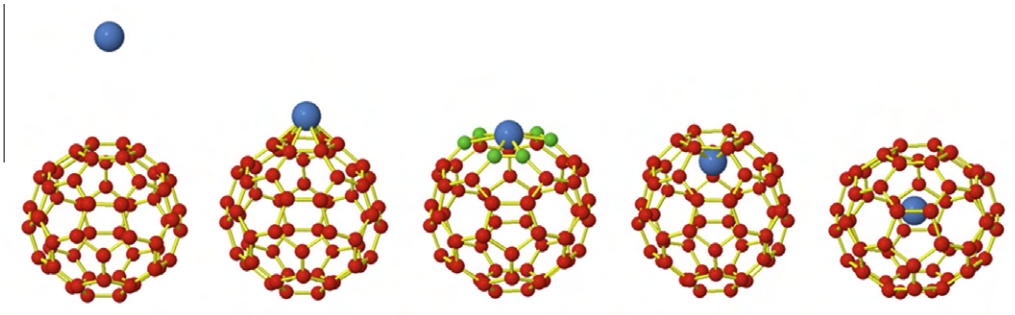

Fig. 2 – Formation mechanism of the incarfullerene $Ni@C_{60}$ for a 5 eV Ni-impact on the center of a hexagon of the buckyball. The color coding corresponds to the color coding in Fig. 1. (For interpretation of the references to color in this figure legend, the reader is referred to the web version of this article.)

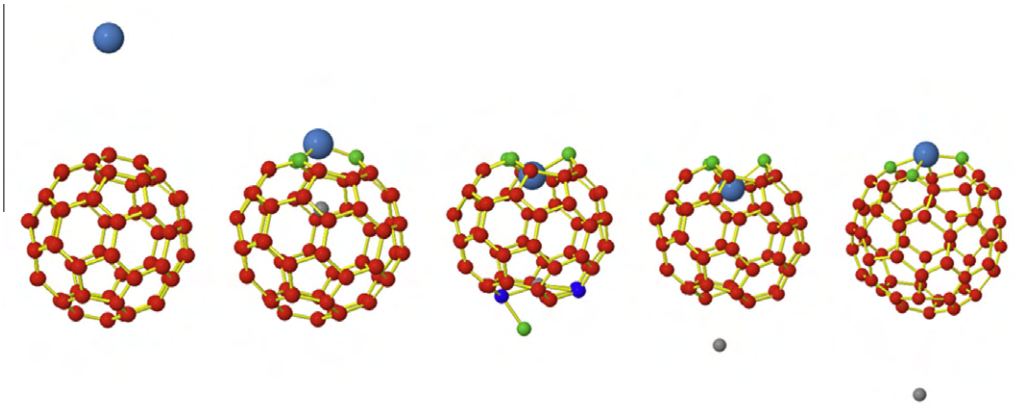

Fig. 3 – Formation mechanism of the heterofullerene $C_{59}Ni$ for a 35 eV Ni-impact on top of an atom of the buckyball. The color coding corresponds to the color coding in Fig. 1. (For interpretation of the references to color in this figure legend, the reader is referred to the web version of this article.)

binds with the three C-atoms that were initially connected to the targetted C-atom. This targetted C-atom is replaced by the Ni-atom, leading to the formation of the heterofullerene $C_{59}Ni$. The resulting cage structure has the characteristic drop shape typically seen for heterofullerenes. This leads to the two Ni–C(6,5) bonds of 1.82 Å and one Ni–C(6,6′) bond of 1.79 Å. These values are comparable to the values of 1.84 Å and 1.81 Å, respectively, by [25], 1.88 Å and 1.86 Å, respectively, by [26], and 1.87 Å and 1.85 Å, respectively, by [24]. The drop shape is further characterized by the deviation from planarity, which is calculated to be 56.8°. The shortest and longest C–C(6,5) bonds are calculated to be 1.43 Å and 1.46 Å, respectively, to be compared to the reported values of 1.45 Å and 1.49 Å, respectively. Likewise, the shortest and longest C–C(6,6) bonds are calculated to measure 1.38 Å and 1.40 Å, respectively, to be compared to be values reported by Sparta et al. [24] of 1.41 Å and 1.42 Å, respectively.

4. Summary and conclusions

In summary, we have performed self-consistent DFT molecular dynamics simulations to explore the possible dynamical formation mechanisms of Ni-doped fullerenes in an ion implantation setup as a function of ion implantation energy and impact location. NiC_{60} is found to be formed by either a surface sticking process or a push-through mechanism. Incarfullerenes can be formed by ring opening upon impingement and subsequent ring closure. Finally, our calculations also demonstrate the formation of the heterofullerene $C_{59}Ni$ by replacement of a C-atom from the structure by the impinging Ni-atom, and the ejection of a second carbon atom by the initially Ni-replaced C-atom. The presented results demonstrate the applicability of an ion implantation source to produce externally doped fullerenes, heterofullerenes, and incarfullerenes.

Acknowledgments

E. Neyts acknowledges the FWO-Flanders (Fund for Scientific Research-Flanders) for the financial support. A. Maeyens is indebted to the Institute for the Promotion of Innovation through Science and Technology in Flanders (IWT-Vlaanderen) for the financial support. The authors also gratefully acknowledge the financial support from the Prime Minister's Office through IAP VI and from IMEC, as well as calculation support of the core facility CALCUA, provided by the University of Antwerp.

REFERENCES

[1] Heath JR, O'Brian SC, Zhang Q, Liu Y, Curl RF, Tittel FK, et al. Lanthanum complexes of spheroidal carbon shells. J Am Chem Soc 1985;107(25):7779–80.
[2] Funasaka H, Sakurai K, Oda Y, Yamamoto K, Takahashi T. Magnetic properties of $Gd@C_{82}$ metallofullerene. Chem Phys Lett 1995;232(3):273–7.
[3] Wilson LJ. Medical applications of fullerenes and metallofullerenes. Electrochem Soc Interface 1999;8(4):24–8.
[4] Bakry R, Vallant RM, Najam-ul-Haq M, Rainer M, Szabo Z, Huck CW, et al. Medicinal applications of fullerenes. Int J Nanomed 2007;2(4):639–49.
[5] Shinohara H. Endohedral metallofullerenes. Rep Prog Phys 2000;63(6):843–92.
[6] Loboda O, Jensen VR, Borve KJ. Multiple additions of palladium to C_{60}. Fullerenes Nanotubes Carbon Nanostruct 2006;14(2–3):365–71.
[7] Lu G, Deng K, Wu H. Geometric and electronic structures of metal-substitutional fullerene $C_{59}Sm$ and metal-exohedral fullerenes $C_{60}Sm$. J Chem Phys 2006;124(5):054305,1–5.
[8] Vostrowsky O, Hirsch A. Heterofullerenes. Chem Rev 2006;106:5191–207.
[9] Wan Z, Christian JF, Anderson SL. Collision of Li^+ and Na^+ with C_{60} – insertion, fragmentation, and thermionic emission. Phys Rev Lett 1992;69(9):1352–5.
[10] Wan Z, Christian JF, Basir Y, Anderson SL. Collision of alkali ions with C_{60}/C_{70} – insertion, thermionic emission, and fragmentation. J Chem Phys 1993;99(8):5858–70.
[11] Christian JF, Wan Z, Anderson SL. $Ne^+ + C_{60}$ – the dynamics of charge and energy transfer, fragmentation, and endohedral complex-formation. J Chem Phys 1993;99(5):3468–79.
[12] Basir Y, Wan Z, Christian JF, Anderson SL. Ion beam studies of atomic ion collisions with C_{60} – chemistry at surface,

substitutional, and endohedral sites. Int J Mass Spectrom Ion Processes 1994;138:173–85.
[13] Basir Y, Anderson SL. Collisions of rare gas ions with C_{60}: endohedral formation, energy transfer, and scattering dynamics. J Chem Phys 1997;107(20):8370–9.
[14] Tellgmann R, Krawez N, Lin SH, Hertel IV, Campbell EEB. Endohedral fullerene production. Nature 1996;382(6590):407–8.
[15] Campbell EEB, Tellgmann R, Krawez N, Hertel IV. Production and LDMS characterisation of endohedral alkali–fullerene films. J Phys Chem Solids 1997;58(11):1763–9.
[16] Watanabe S, Ishioka NS, Sekine T, Osa A, Koizumi M, Shimomura H, et al. Production of endohedral Xe-133–fullerene by ion implantation. J Radioanal Nucl Chem 2003;255(3):495–8.
[17] Kaplan A, Bekkerman A, Tsipinyuk B, Kolodney E. The formation and ejection of endohedral $Cs@C_{60}^+$ by low energy collisions (35–220 eV) of Cs^+ ions with surface absorbed C_{60} molecules. J Chem Phys 2002;117(7):3484–91.
[18] Huang H, Ata M, Yoshimoto Y. $Cu@C_{60}$ formation in rf-plasma and ring-current induced magnetism of C_{60}. Chem Commun 2004;10:1206–7.
[19] Branz W, Billas IML, Malinowski N, Tast F, Heinebrodt M, Martin TP. Cage substitution in metal–fullerene clusters. J Chem Phys 1998;109(9):3425–30.
[20] Kong QY, Shen YF, Zhao L, Zhuang J, Qian SX, Li YF, et al. Formation of various types of metallofullerenes by laser ablation of externally doped fullerenes $C_{60}M_x$ (M = Sm, Pt, Ni, La, Y, and Rh). J Chem Phys 2002;116(1):128–36.
[21] Kong Q, Zhuang J, Li X, Cai R, Zhao L, Qian S, et al. Formation of metallofullerenes by laser ablation of externally doped fullerenes $C_{60}M_x$ (M = Sm, Pt, and Ni). Appl Phys A Mater Sci Process 2002;75(3):367–74.
[22] Ohtsuki T, Ohno K, Shiga K, Kawazoe K, Maruyama Y. Systematic study of foreign-atom-doped fullerenes by using a nuclear recoil method and their MD simulation. J Chem Phys 2000;112(6):2834–42.
[23] Akiyama K, Sueki K, Haba H, Tsukada K, Asai M, Yaita Y, et al. Production and characterization of actinide metallofullerenes. J Radioanal Nucl Chem 2003;255(1):155–8.
[24] Sparta M, Jensen VR, Børve KJ. Structure and stability of substitutional metallofullerenes of the first-row transition metals. Fullerenes Nanotubes Carbon Nanostruct 2006;14(2–3):269–78.
[25] Changgeng D, Jinlong Y, Xiangyuan C, Chan CT. Geometric and electronic structures of metal-substituted fullerenes $C_{59}M$ (M = Fe, Co, Ni, and Rh). J Chem Phys 1999;111:8481–5.
[26] Alemany MMG, Diéguez O, Rey C, Gallego LJ. A density-functional study of the structures and electronic properties of $C_{59}Ni$ and $C_{60}Ni$ clusters. J Chem Phys 2001;114(21):9371–4.
[27] Andriotis AN, Menon M. Geometry and bonding in small $(C_{60})_nNi_m$ clusters. Phys Rev B 1999;60(7):4521–4.
[28] Yamaguchi Y, Maruyama S. A molecular dynamics study on the formation of metallofullerene. Eur Phys J D 1999;9(1–4): 385–8.
[29] Neyts EC, Bogaerts A. Formation of endohedral $Ni@C_{60}$ and exohedral $Ni–C_{60}$ metallofullerene complexes by simulated ion implantation. Carbon 2009;47(4):1028–33.
[30] Ordejón P, Artacho E, Soler JM. Self-consistent order-N density-functional calculations for very large systems. Phys Rev B 1996;53(16):10441–4.
[31] Soler JM, Artacho E, Gale JD, García A, Junquera J, Ordejón R, et al. The SIESTA method for ab initio order-N materials simulation. J Phys Condens Matter 2002;14(11):2745–79.
[32] Perdew JP, Zunger A. Self-interacting correction to density-functional approximations for many-electron systems. Phys Rev B 1981;23(10):5048–79.
[33] Troullier N, Martins JL. Efficient pseudopotentials for plane-wave calculations. Phys Rev B 1991;43(3):1993–2006.
[34] Troullier N, Martins JL. Efficient pseudopotentials for plane-wave calculations: 2. Operators for fast iterative diagonalization. Phys Rev B 1991;43(11):8861–9.
[35] Hirata T, Otomo Y, Hatakeyama R. Production and control of La plasma and application to fullerene-related material process. Thin Solid Films 2002;407(1–2):32–7.